Article

Hydrogen Peroxide Activation with Sulfidated Zero-Valent Iron for Synchronous Removal of Cr(VI) and BPA

Haibo Ling [1,2], Xiaowei Zhu [1], Ting Zhou [1], Fan Su [1], Jiangkun Du [1,*] and Jianguo Bao [1,*]

1   School of Environmental Studies, China University of Geosciences, Wuhan 430074, China; zoesling@163.com (H.L.); 1219144@mail.dhu.edu.cn (X.Z.); 18202721355@163.com (T.Z.); sufan0605@126.com (F.S.)
2   Hubei Provincial Academy of Eco-Environmental Sciences, Wuhan 430072, China
*   Correspondence: dujk@cug.edu.cn (J.D.); bjianguo@cug.edu.cn (J.B.)

Abstract: In this work, the synchronous removal of Cr(VI) and bisphenol A (BPA) in a heterogeneous Fenton process with sulfidated nanoscale zero-valent iron (S-nZVI) as the reductant and catalyst was systematically evaluated. Compared to other systems including S-nZVI or H_2O_2 alone, a simultaneous BPA degradation and Cr(VI) removal could be achieved in the S-nZVI/H_2O_2 system at an optimum pH of 3. It was, interestingly, found that 7.8% of BPA and 98.2% of Cr(VI) were removed within 60 min in presence of S-nZVI alone, whereas, correspondingly, 98.2% of BPA and 96.9% of Cr(VI) were eliminated in the S-nZVI/H_2O_2 system. Specifically, humic acid (HA) and $H_2PO_4^-$ inhibited the deterioration of BPA but posed no significant effect on Cr(VI) removal. NO_3^- had a slight lifting effect on the removal of BPA and Cr(VI), while HCO_3^- showed a relatively weak prohibition. Experiments with EPR and radical probe tests also provide direct evidence that hydroxyl radicals was monitored in the S-nZVI/H_2O_2 system, which not only degraded BPA but also inhibited the reduction of Cr(VI). It could not be ignored that FeS accelerated Fe^0 corrosion to release Fe^{2+}. In, addition, Fe^0, Fe^{2+} and S^{2+} could react with Cr(VI) while the most of produced Cr(III) was co-precipitated in the form of $Cr_xFe_{1-x}OOH$ film. The study confirmed that it was feasible for S-nZVI/H_2O_2 system to remove synchronously organic pollutants and heavy metal.

Keywords: sulfur-modified zero-valent iron; hexavalent chromium; bisphenol A; synchronous removal; Fenton reaction

1. Introduction

The co-contamination of heavy metals and refractory organic compounds in wastewater have become an urgent environmental problem nowadays. One typical example is that chromate (Cr(VI)) is commonly present together with organic pollutants in industrial waste of metal finishing, wood preserving, petroleum refining, and even in contaminated fields. It is well known that Cr(VI) is acutely toxic, carcinogenic and mutagenic to living organisms. In contrast, Cr(III) is less toxic and can be easily removed through precipitation [1]. The effective transformation of Cr(VI) into Cr(III) is a preferred method for reducing contamination. However, the reduction of Cr(VI) and the oxidation of organic pollutants seems theoretically contradictory, making this kind of wastewater difficult to treat [2,3]. Thus, efficient and simultaneous removal of Cr(VI) and organic pollutants is of great significance for water remediation.

Nanoscale zero-valent iron (nZVI) is a versatile material with high reductive capacity ($E^0 = -0.44$ V). Due to this strong reductivity, nZVI has shown attractive potential in the ex/in situ transformation of Cr(VI) to the less toxic Cr(III) [4]. Ferrous and ferric ions, as corrosion products of nZVI, would be sacrificed to precipitate with Cr(III) to form insoluble minerals, making nZVI a promising material for Cr(VI)-bearing wastewater treatment. In addition, the Fenton or Fenton-like reactions are attractive for the removal of recalcitrant contaminants from aqueous solutions via the generation of powerful radicals

(such as $\cdot OH$ and $SO_4 \cdot^-$) from the disintegration of oxidants (such as H_2O_2 and persulfate) with Fe^{2+} oxidized to Fe^{3+}, as per Equations (1) and (2) [5]. Typically, iron acts as the catalyst to activate H_2O_2 or persulfate (PS, $S_2O_8^{2-}$) to generate into radicals, which exhibit strong oxidizing capability and are capable of degrading most of the organic pollutants to CO_2, H_2O, or intermediate products such as organic acids with a series of rapid chain reactions [6]. In particular, the dissolved Fe^{2+} is essential for radical production, and nZVI is widely used as a source of in situ Fe^{2+} precursor in heterogeneous Fenton-like systems [7,8]. Compared to the homogeneous Fenton reaction, the nZVI-Fenton reaction can run in a wider pH range because of the fast circulation of Fe^{2+}/Fe^{3+} on the Fe^0 surface [9,10]. With these advantages, the nZVI-based Fenton-like reaction is expected to be an efficient means of wastewater purification.

$$Fe^{2+} + H_2O_2 \rightarrow Fe^{3+} + OH^- + \cdot OH \tag{1}$$

$$Fe^{2+} + S_2O_8^{2-} \rightarrow Fe^{3+} + SO_4^{2-} + SO_4 \cdot^- \tag{2}$$
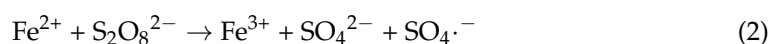
In a typical Fenton-like process with nZVI, the reducing capacity of Fe^0 was used to activate H_2O_2 or persulfate with the formation of $\cdot OH$ or $SO_4 \cdot^-$ for the oxidation of organic pollutants. In this sense, most studies have only focused on the oxidation of organic pollutants, ignoring cases of co-contamination. In fact, nZVI-based Fenton-like systems have the potential to remove both heavy metals and organic pollutants in a single system [11,12]. Yin et al. studied the removal of coexisting Cr(VI) and 4-chlorophenol by reducing Cr(VI) in a first step with subsequent H_2O_2 oxidation. They found that 100% of Cr(VI) could be reduced by nZVI within 20 min, and the subsequent addition of H_2O_2 initiated a Fenton reaction for 4-CP degradation [13]. Yang et al. found that the total dissolved copper (TCu) and methylene blue (MB) could be removed together in the ZVI/H_2O_2 system [14]. In addition to the $nZVI/H_2O_2$ system, the simultaneous removal of phenol and Cr(VI) could be achieved using a system containing bentonite-supported nZVI (B-nZVI) and persulfate, as reported by Diao et al. [15]. A positive increase in dissolved Fe^{2+} was found throughout persulfate decomposition, and $SO_4 \cdot^-$ was identified as acting toward phenol degradation, while B-nZVI was responsible for Cr(VI) [16]. However, the previous studies ignored the interaction effect between Cr(VI) and organic pollutants, and the efficiency and mechanism of their simultaneous removal in the $nZVI/H_2O_2$ Fenton-like system are still unclear.

In this study, the synchronous removal of Cr(VI) and bisphenol A (BPA) was evaluated in both H_2O_2 and persulfate oxidation systems. A sulfidated nanoscale zero-valent iron (S-nZVI) was chosen as the activator of the reaction system, because it has been reported to show significantly better efficiency with respect to Cr(VI) removal [17]. To elucidate the interaction effects between Cr(VI) and BPA, the effect of pH, H_2O_2 and catalyst dosage were investigated. The possible mechanism of pollutant elimination was further investigated by radical analysis and material characterization.

2. Materials and Methods

All chemicals, including ferrous sulfate ($FeSO_4 \cdot 7H_2O$), sodium sulfide ($Na_2S \cdot 9H_2O$), sodium borohydride ($NaBH_4$), absolute ethyl alcohol, sodium sulfate hydrate ($Na_2SO_4 \cdot 10H_2O$) potassium dichromate ($K_2Cr_2O_7$), bisphenol A (BPA), hydrogen peroxide (H_2O_2), and 1,10-phenanthroline, were purchased from Sinopharm Chemical Reagent Co., Ltd. (Shanghai, China). Deionized water (≥ 18.0 $M\Omega$ cm^{-1}) was deoxygenated by high-purity nitrogen purging for 1 h before use.

2.1. Preparation nZVI and S-nZVI

nZVI and S-nZVI nanoparticles were prepared according to our previous research [17]. Firstly, 50 mL of $NaBH_4$ (0.036 mol/L) and 100 mL of $FeSO_4 \cdot 7H_2O$ (0.018 mol/L) was added dropwise into a three-neck flask under N_2 protection. Then, the resulting nZVI

suspensions in the three-neck flask were magnetically separated and rinsed with anaerobic water and ethanol three times.

To obtain S-nZVI, prepared $FeSO_4 \cdot 7H_2O$ solution was mixed with nZVI to obtain uniform dispersion, and then Na_2S solution was added dropwise into the flask and the mixture was stirred continuously for 20 min. Finally, the zero-valent iron was magnetically separated and rinsed as described above, and vacuum-dried at 50 °C overnight. The whole preparation process was performed under a N_2 atmosphere.

2.2. Experimental Procedures

The synchronous Cr(VI) sequestration and BPA degradation were conducted in a 250 mL beaker with 100 mL solution open to the atmosphere. The initial concentration of Cr(VI) and BPA was the same: 5 mg/L. Unless otherwise specified, an aliquot of stock solution of H_2O_2 (0.2 mmol/L) and S-nZVI (50 mg/L) was sequentially injected as a trigger for the reaction. At specific time intervals, 2 mL of samples were periodically collected and immediately mixed with 2 mL of ethanol to terminate the reaction, then filtered with 0.22 μm PTFE membrane filters for further analysis. The effects of initial pH, oxidant dosage, and catalyst dosage on synchronous removal of BPA and Cr(VI) by S-nZVI/H_2O_2 system were investigated. Specifically, latent co-existing water anions (HCO_3^-, $H_2PO_4^-$, NO_3^-) and humic acid (HA) were also examined to obtain a better understanding of their adaptability in an aquatic environment. All experiments were conducted in duplicate.

To investigate the free radical species, ethanol (2 mmol/L) was added as a radical scavenger and 5,5-dimethyl-1-pyrroline-N-oxide (DMPO) was used as a spin trap agent for electron paramagnetic resonance (EPR) analysis (EMX-8/2.7C, Bruker, Germany) [18]. Synchronous removal of BPA and Cr(VI) with or without *o*-phenanthroline (*o*-phenanthroline: S-nZVI = 10:1) was performed to investigate the effect of Fe(II).

2.3. Analysis

The surface morphologies and element mappings of the S-nZVI were observed by scanning electron microscopy (SEM) (ZEISS Ultra 55., Germany) combined with energy dispersive X-ray spectroscopy (EDX). The mineralogical identity and structures were determined by a D/Max-IIIA Powder X-ray Diffractometer (XRD) (Rigaku Corp., Tokyo, Japan) equipped with Cu–K_α radiation. The surface compositions of the S-nZVI were determined by X-ray photoelectron spectroscopy (XPS) (Thermo-VG Scientific ESCALB-250 with Al–$K\alpha$ radiation).

The concentration of BPA was measured by high-performance liquid chromatography (HPLC, LBP, 3000, RIGOL, Beijing, China). Cr(VI) was measured using a UV-vis spectrometer for the 1,5-diphenylcarbazide colorimetric method at a wavelength of 544 nm, and the concentration of total chromium was determined by flame atomic adsorption spectrometry (Flame-AAS, 240, Agilent, Santa Clara, CA, USA). Cr(III) was identified by calculating the difference between the total chromium concentration and Cr(VI). Hydrogen peroxide was examined by a UV-vis spectrophotometer at 400 nm after coloration with $Ti(SO_4)_2$. The concentration of ferrous ions was measured by the *o*-phenanthroline method at wavelength of 510 nm. The concentration of total iron ions was measured by adding hydroxylamine hydrochloride to reduce ferric ions into ferrous ions. Total organic carbon (TOC) was determined by TOC analyzer (Liqui TOC II).

3. Results and Discussion

3.1. Characterization of S-nZVI

The surface morphology and element distribution of pristine S-nZVI was characterized by SEM-EDX as well as TEM. As shown in Figures S1 and S2, the spherical particles of Fe^0 are covered with a thin layer of micrometer-sized material, which can be attributed to FeS. In addition, peaks of Fe and S elements were observed in the EDS mapping (Figure S1c). As shown in Figure S3, both S-nZVI and nZVI shows shrill 2θ peaks at 44.79°, which correspond to the [110] directions of α-Fe, indicating the high purity and crystallinity of

Fe^0. Moreover, the diffraction peak of S-nZVI was much lower than that of nZVI, because the Fe^0 core was encapsulated by a coverage of amorphous FeS. The above characterization indicates that S-nZVI is a core–shell structure with a coverage of FeS.

3.2. Cr(VI) and BPA Removal in Different Systems

The different systems on synchronous removal of BPA and Cr(VI) were investigated. As shown in Figure 1a, only 8.6–11.3% of BPA was removed when H_2O_2 or nZVI or S-nZVI were used individually during the reaction. However, the removal rates of BPA by nZVI/H_2O_2 and S-nZVI/H_2O_2 systems were 97.7% and 98.5% after 20 min, respectively, indicating that the oxidative role of H_2O_2 should be activated to produce reactive species responsible for the degradation of BPA (Equations (3) and (4)) [19]. Noteworthily, the coupling of S-nZVI with H_2O_2 presented the highest efficiency for the degradation of BPA, and sulfur promotes the nZVI corrosion with generation of more hydroxyl radicals for BPA degradation [20]. Upon the detection of TOC variation (Figure S4), it was found that rapid TOC removal was achieved during the initial stage of the reaction. Then, after 10 min reaction, more TOC was gradually removed, and finally, 67.7% of TOC was eliminated in the S-nZVI/H_2O_2/Cr/BPA system. This result suggests that a considerable amount of BPA can be mineralized to carbon dioxide and water in the reaction. Interestingly, it was observed that 34.9% of Cr(VI) was removed by H_2O_2 alone within 60 min (Figure 1b). As a strong oxidant, $K_2Cr_2O_7$ (E^0 = 1.33 V) can be reduced by H_2O_2 (E^0 = 0.678 V) according to Equation (5) [21]. Furthermore, 22.8% and 28.8% of Cr(VI) were removed by nZVI/H_2O_2 and S-nZVI/H_2O_2 systems after 5 min, respectively, values which were lower than those obtained for nZVI (70.9%) and S-nZVI (76.3%) systems. The reaction rate of Fe^{2+}/H_2O_2 (2.58~3.14 min^{-1}) is much higher than that of Cr(VI) with Fe^{2+} (0.0763~0.1078 min^{-1}), and the produced ·OH could oxidize Cr(III) back to Cr(VI) [22]. Noteworthily, the removal efficiency of Cr(VI) in H_2O_2/S-nZVI system (79.4%) was much higher than that of the H_2O_2/nZVI system (37.5%) after 10 min, indicating the better performance of S-nZVI compared to nZVI (Equations (6)–(8)). After 20–30 min, both H_2O_2/nZVI and H_2O_2/S-nZVI systems achieved over 95% of Cr(VI) removal, close to that obtained by nZVI (97.8%) and S-nZVI (98.2%). The above results clearly suggest that the synchronous removal of BPA and Cr(VI) can be successfully achieved in nZVI-based Fenton-like systems, and S-nZVI performed better than bare nZVI.

$$Fe^{2+} + H_2O_2 \rightarrow Fe^{3+} + \cdot OH + OH^- \tag{3}$$

$$Cr(n) + H_2O_2 \rightarrow Cr(n + 1) + \cdot OH + OH^- \ (n = IV \text{ or } V) \tag{4}$$

$$2HCrO_4^- + 8H^+ + 3H_2O_2 \rightleftharpoons 2Cr_3^+ + 3O_2 + 8H_2O \tag{5}$$

$$S^{2-} + Cr_2O_7^{2-} + 2H^+ \rightarrow SO_3^{2-} + Cr(OH)_3\downarrow + H_2O \tag{6}$$

$$Cr_2O_7^{2-} + 6Fe^{2+} + 14H^+ \rightarrow 6Fe^{3+} + 2Cr^{3+} + 7H_2O \tag{7}$$

$$Cr_2O_7^{2-} + 3Fe^0 + 14H^+ \rightarrow 3Fe^{3+} + 2Cr^{3+} + 7H_2O \tag{8}$$
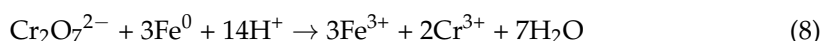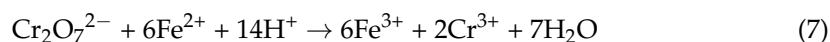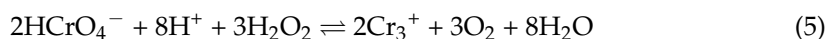
To further detect the interaction of BPA and Cr(VI) in a S-nZVI/H_2O_2 system, the effect of one contaminant on the other contaminant was investigated via batch experiments. For example, the effects of BPA on Cr(VI) removal were studied with different initial concentrations. Figure 1c shows that the degradation efficiency of BPA decreased when Cr(VI) was added into the S-nZVI/H_2O_2 system, because Cr(VI) consumed the reductive Fe species and also reacted with H_2O_2. Therefore, the degradation of BPA was eventually inhibited with increasing dosage of Cr(VI), inactivating more H_2O_2 and decreasing the yield of hydroxyl radicals (Figure 1e). Conversely, the presence of BPA showed no significant inhibitory effect, but rather a positive promotion of Cr(VI) removal (Figure 1d). However, it was noticed that this promotion was not further enhanced with increasing BPA concentration (Figure 1f). The competitive reaction between BPA and H_2O_2 seemed to protect Cr(VI) from oxidation and facilitate its reduction on the S-nZVI surface.
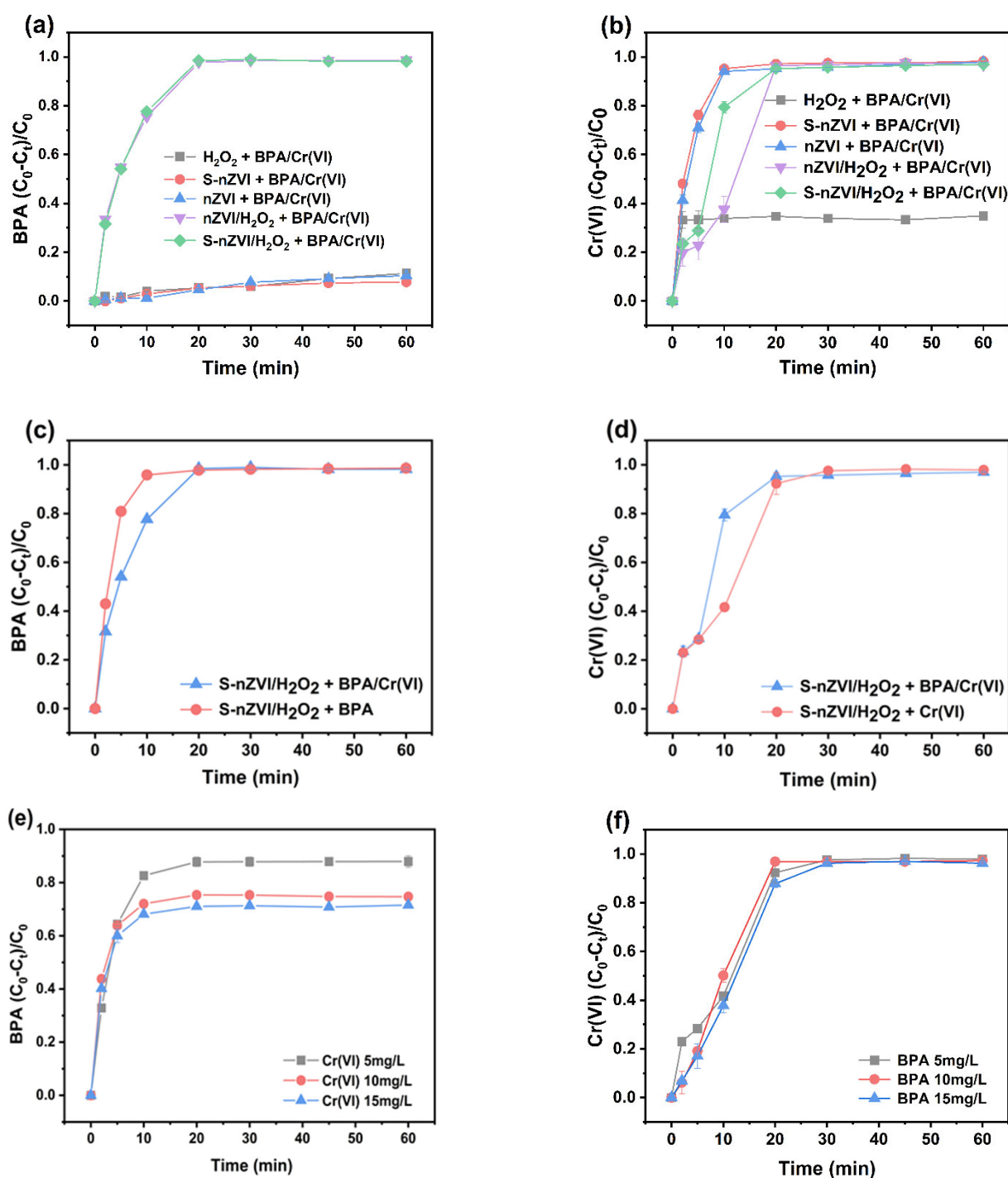
Figure 1. Synchronous removal of (**a**) BPA and (**b**) Cr(VI) in different reaction systems; removal of BPA (**c**) or Cr(VI) (**d**) alone by S-nZVI/H_2O_2; the degradation of BPA under different Cr(VI) concentrations (**e**) and the reduction of Cr(VI) at different BPA concentrations (**f**).

In the past decade, $SO_4 \cdot^-$-based advanced oxidation processes using PS as the oxidant have been studied intensively for wastewater treatment. In comparison with the S-nZVI/PS Fenton-like system, as shown in Figure S5, S-nZVI/H_2O_2 exhibited a significantly higher efficiency in BPA oxidation, indicating a higher oxidation capacity of S-nZVI/H_2O_2 than S-nZVI/PS. Conversely, Cr(VI) seemed to be removed more quickly in the S-nZVI/PS system than in the S-nZVI/H_2O_2 system, implying a lower interference of PS activation on Cr(VI). This result is consistent with that reported by Diao et al., where Cr(VI) removal was negligibly influenced by PS in the nZVI/PS system. However, after 20 min reaction,

the difference between the two reaction schemes was really minor, and was surprisingly uniform after 30 min. The reduction of Cr(VI) after 30 min was over 95%, and achieved equilibrium in the remaining reaction time. Considering the joint removal performance of BPA and Cr(VI), the S-nZVI/H_2O_2 system seemingly showed a more comprehensive potential than S-nZVI/PDS with respect to the treatment of co-contamination of BPA and Cr(VI).

3.3. Effect of pH, Oxidant Dosage, Catalyst Dosage

It was observed that Cr(VI) reduction and BPA oxidation were dependent on varying pH conditions (Figure S6a). Approximately 90% of BPA was removed after 20 min at pH = 3, whereas there was almost no obvious BPA degradation at pH 7.0 and 9.0, indicating that BPA removal increased with decreasing initial pH value, which might be attributed to the generation of more hydroxyl radicals by S-nZVI/H_2O_2 in acidic conditions [23]. It was observed that 97.8%, 54.6%, 57.6%, 53.1% and 45.5% of Cr(VI) removal were obtained at pH values of 3, 4, 5, 7 and 9, respectively (Figure S6b). This suggests that acidic conditions favor Cr(VI) removal. More indissoluble Fe^{3+} hydroxide was precipitated with Cr(III) to form a Fe-Cr hydroxide layer under neutral or alkaline conditions [17]. These precipitates on nZVI surface occupy active sites, limiting Fe^{2+} release, and retarding electron transfer from S-nZVI to Cr(VI) [24]. In addition, the oxidation potential of ·OH decreased along with the increase in solution pH, from 2.65–2.80 V at pH 3.0 to 1.90 V at pH 7.0, as previously reported [19]. Nevertheless, some researchers have reported that Cr(VI) sequestration by nano-FeS_2 increases notably with an increase in suspension pH from 5.0 to 9.0 [25]. This is because S^{2-} plays a primary role in the reactive surface of nano-FeS_2, having higher nucleophilicity in an alkaline solution, and may enhance the reduction of Cr(VI). In this work, Cr(VI) was completely removed at pH 3, while approximately 50% Cr(VI) removal was obtained under other pH conditions, indicating that acidic conditions (pH = 3) were conducive to Cr(VI) removal.

The influence of oxidant dosage on the synchronous removal of Cr(VI) and BPA in the S-nZVI/H_2O_2 system is depicted in Figure S6c,d. The BPA removal rate increased from 88.5% to 98.0% after 20 min when the amount of oxidant added to the system was increased from 0.2 mmol/L to 0.4 mmol/L (Figure S6c). These results conclusively demonstrate the key role played by H_2O_2 in the generation of ·OH for BPA degradation in this system. Interestingly, despite there being no obvious difference observed in BPA removal when the H_2O_2 dosages were in the range of 0.4 to 0.8mmol/L, the reaction constant decreased from 0.298 min^{-1} to 0.209 min^{-1}. In fact, excessive H_2O_2 could cause the release of a mass of ·OH, resulting in the self-quenching of hydroxyl radicals, as shown in Equations (9) and (10) [25].

$$H_2O_2 + OH\cdot \rightarrow H_2O + \cdot O_2H \qquad (9)$$

$$\cdot O_2H + OH\cdot \rightarrow H_2O + O_2 \qquad (10)$$
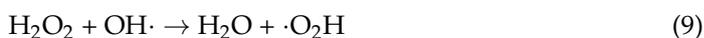
As shown in Figure S6d, when the H_2O_2 dosages exceeded 0.4 mmol/L, Cr(VI) removal rapidly increased during the first 2 min, then the amount of Cr(VI) gradually decreased, but an increase in Cr(VI) removal was observed after 30 min, meaning that Cr(VI) removal decreased with increasing H_2O_2 dosage. This may be due to the generation of hydroxyl radicals with increasing H_2O_2 dosage, causing Cr(III) to be reconverted into Cr(VI) and the competition between excess H_2O_2 and Fe^{2+}, which could quickly remove Cr(VI). Therefore, the larger the oxidant dosage, the slower the removal rate of Cr(VI) at H_2O_2 concentrations higher than 0.4 mmol/L. In addition, the dosage of S-nZVI is also a vital control variable for BPA and Cr(VI) removal. As shown in Figure S6e,f, the increment of S-nZVI significantly accelerated the synchronous removal of BPA and Cr(VI) when increasing the S-nZVI dosage from 0.02 to 0.15 g/L. Specifically, the reaction kinetics constant of BPA degradation increased from 0.088 min^{-1} to 0.276 min^{-1}. Increasing the dosage of S-nZVI provided more active sites for not only Fenton-like catalysis, but also Cr(VI) sequestration. In addition, the ultimate removal rates of BPA and Cr(VI) were similar when

the S-nZVI dosage was increased from 0.05 to 0.15 g/L. Hence, considering the cost and practical application of S-nZVI, 0.05 g/L of it was chosen for the subsequent experiments.

3.4. Effect of Water Matrices

Humic acid (HA) and coexisting water anions (including HCO_3^-, NO_3^-, $H_2PO_4^-$) are widely present in the environment and interfere with the process of environmental restoration. As shown in Figure 2a, the removal of BPA decreased from 97.7% to 63.7% when HA concentration was increased from 0 to 50 mg/L. Since humic acid is a kind of organic substance, it competes with BPA to quench ·OH, resulting in a decrease in BPA degradation rate [26]. Additionally, humic acid might integrate with surface iron (such as Fe^{2+}, Fe^{3+} and $Fe(0)$) to form dissolved Fe–humate complexes, causing a loss of reducing substances as well as decreasing the removal efficiency of BPA [27]. However, when a small amount of HA (5 mg/L) was spiked into the reaction solution, almost no influence on Cr(VI) removal was observed (Figure 2b). In particular, humic acid also acts as an additional adsorbent and electron transfer mediator at tiny concentrations due to its multiple functional groups [28], which ultimately offset the negative impact of highly concentrated HA for Cr(VI) removal.
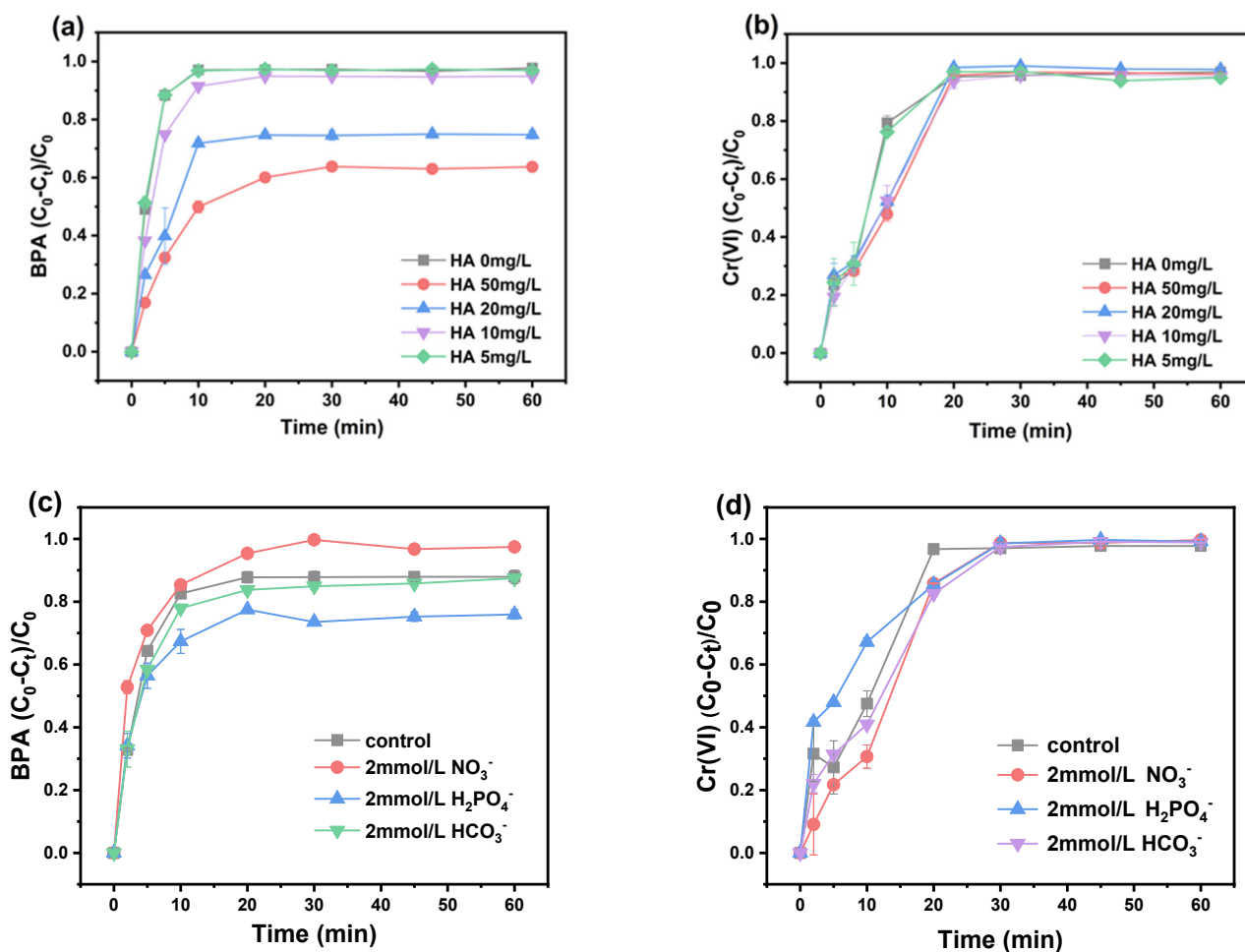

Figure 2. Effect of (**a**,**b**) humic acid and (**c**,**d**) inorganic anions on synchronous removal of BPA and Cr(VI) by S-nZVI.

As presented in Figure 2c,d, the removal rate of both BPA and Cr(VI) by S-nZVI/H_2O_2 was significantly influenced in the presence of NO_3^- and $H_2PO_4^-$, but slightly suppressed by HCO_3^-. The slight inhibition of HCO_3^- here could be because of its reaction with Fe^{2+} to form $FeCO_3$ or hydroxyl carbonate, which attached to the surface of S-nZVI, resulting

in a decrease in iron ions and reactive sites [28]. However, in the presences of NO_3^-, the removal efficiency of BPA increased from 98.9% to 99.7%, while the initial removal efficiency of Cr(VI) increased from 95.7% to 98.7% in 30 min. This is probably because NO_3^- competes with Cr(VI) for reactive sites in S-nZVI and produces more Fe(II) at the solid–liquid interface (as per Equations (11) and (12)) [20]. Moreover, $H_2PO_4^-$ showed a different effect, wherein the rate of BPA removal decreased from 98.2% to 75.9% while the Cr(VI) removal increased from 96.9% to 99.1%. Firstly, this could be because $H_2PO_4^-$ can complex with Cr(VI) to form a water-soluble complex [29], preventing the formation of a zero-valent iron surface passivation layer and improving the removal of Cr(VI). Secondly, $H_2PO_4^-$ is a typical radical scavenger, thus inhibiting the degradation of BPA [30].

$$Fe^0 + NO_3^- + 2H^+ \rightarrow Fe^{2+} + H_2O + NO_2^- \tag{11}$$

$$4Fe^0 + NO_3^- + 10H^+ \rightarrow 4Fe^{2+} + 3H_2O + NH_4^+ \tag{12}$$

3.5. Proposed Reaction Mechanism

Accordingly, it can be deduced that BPA was degraded by activating H_2O_2 with S-nZVI, but the removal of Cr(VI) was achieved by ferrous on S-nZVI surface. To clarify the role of Fe(II) on BPA and Cr(VI) elimination, *o*-phenanthroline was added into the reaction system as a Fe(II) shielding agent. As shown in Figure 3a,b, the removal of Cr(VI) and BPA was significantly inhibited after adding *o*-phenanthroline. The BPA removal rate decreased from 97.7% to 29.1%, and the Cr(VI) removal rate decreased from 97.8% to 17.6%, implying that Fe(II) not only participated in the Fenton reaction as an activator of H_2O_2, but also reduced Cr(VI) into Cr(III) as an electron donor [31]. In addition, the H_2O_2 use rates were determined for different systems as shown in Figure 3c. It can be observed that H_2O_2 was completely used in 60 min for the H_2O_2/S-nZVI/BPA/Cr system, while 82.4% and 68.8% were achieved for the H_2O_2/S-nZVI/BPA and H_2O_2/S-nZVI/Cr(VI) systems, respectively. Moreover, the use of H_2O_2 also reached 64.7% when S-nZVI was not added, due to the catalysis of chromium, which is consistent with the results in Figure 1, suggesting that H_2O_2 could be decomposed in presence of Cr(VI) via a redox process (Equations (14) and (15)). Both Fe and Cr species are able to react with H_2O_2, thus consuming more H_2O_2 than systems with a single contaminant [32].

$$HCrO_4^- + 2H_2O_2 + H^+ \rightleftharpoons CrO(O_2)_2 + 3H_2O \tag{13}$$

$$2CrO(O_2)_2 + 6H^+ \rightleftharpoons 2Cr^{3+} + 3O_2 + H_2O_2 + 2H_2O \tag{14}$$
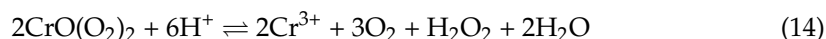
The catalytic activation of H_2O_2 is most likely to produce ·OH via a Haber-Weiss-type reaction [33]. As a typical ·OH quencher, ethanol was used to identify the presence of ·OH in the present reaction system, and the removal efficiencies of BPA with or without ethanol were evaluated. As observed in Figure 3d, 14.22% of BPA was removed after 20 min in the presence of ethanol, whereas the removal rate of BPA was 89.92% without ethanol, suggesting an obvious inhibitory effect of ethanol on BPA degradation. In contrast, no significant difference was observed in Cr(VI) removal with scavenger (Figure 3e). The EPR technique with 5,5-dimethyl-1-pyrrolidine-*N*-oxide (DMPO) as a spin-trapping agent was used to further identify the production of ·OH in the S-nZVI/H_2O_2 system. As shown in Figure S7, there exists a characteristic peak with a peak height ratio of 1:2:2:1, and the signal intensity of DMPO-OH increased in first 2 min but then gradually decreased due to the consumption of H_2O_2. These results suggest that ·OH was the principal species responsible for BPA degradation in the S-nZVI/H_2O_2/Cr(VI)/BPA reaction system.
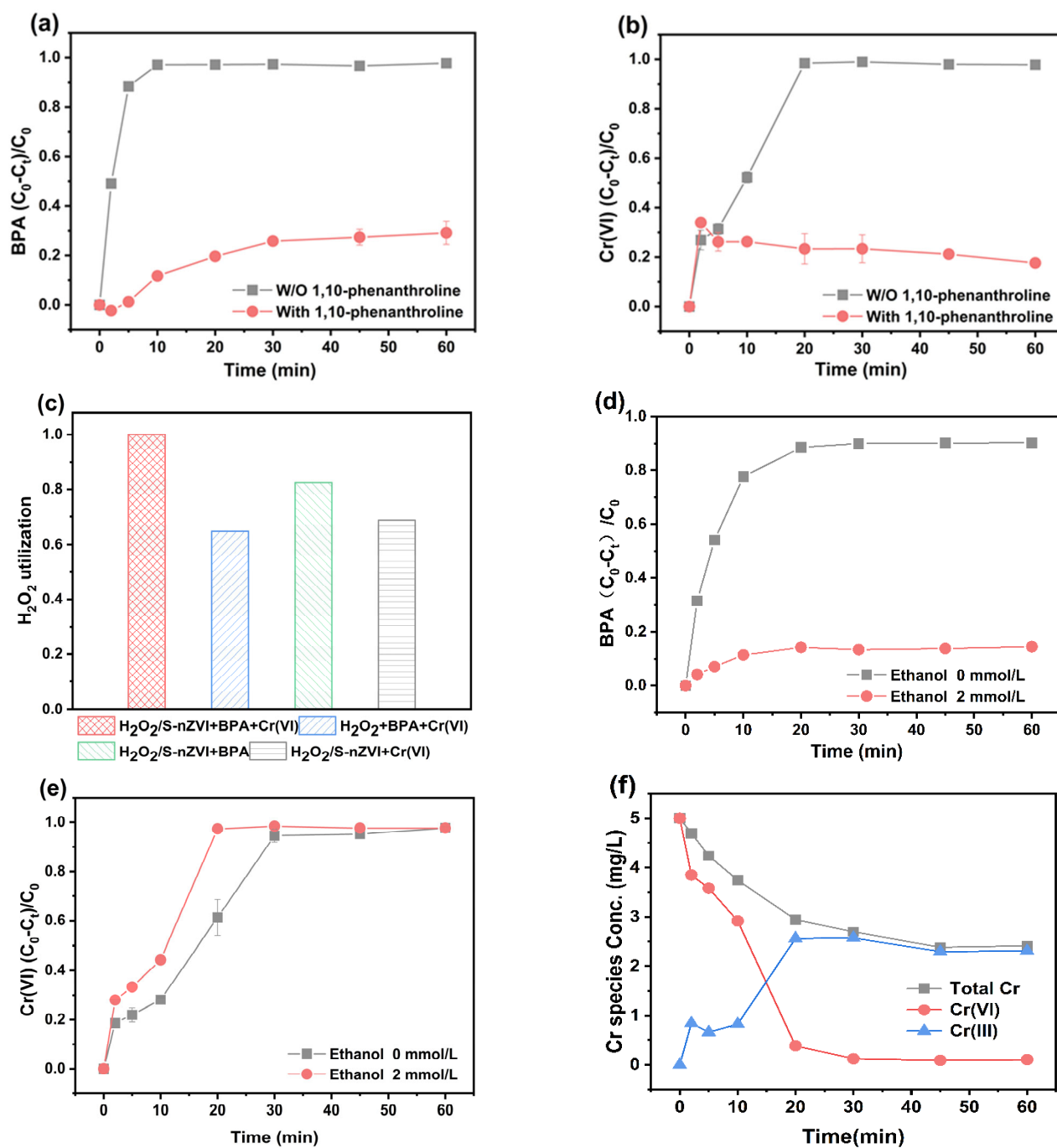
Figure 3. The synchronous removal of (**a**) BPA and (**b**) Cr(VI) by S-nZVI/H_2O_2 with/without the presence of o-phenanthroline; (**c**) the use rate of hydrogen peroxide in different systems; the synchronous removal of (**d**) BPA, and (**e**) Cr(VI) by S-nZVI/H_2O_2 with/without the presence of ethanol; (**f**) the concentration of Cr species in the solution.

The transformation of Cr(VI) is important for detoxification, and the species of aqueous Cr varies with S-nZVI reduction and ·OH oxidation. As presented in Figure 3f, the concentration of total Cr in solution decreased along with the elimination of Cr(VI). Aqueous chromium was continuously reduced and immobilized by S-nZVI, which is consistent with previous studies reporting that Fe^0 corrodes and yields the iron (hydro)oxides to remove heavy metals throguh adsorption and co-precipitation [2]. However, it is worth noting that the concentration of total Cr at every time point is higher than that of Cr(VI). This result is different from that reported in our previous study, which indicated that the total

Cr and Cr(VI) displayed almost same removal tendency [17]. This is because a significant portion of Cr(VI) was transformed to Cr(III) through the reaction with H_2O_2, and therefore was not captured by S-nZVI [34]. This phenomenon is evidenced by the variation of Cr species. For example, the concentration of Cr(III) decreased from 0.84 mg/L to 0.66 mg/L in 5 min, which could be due to the reversible conversion of Cr species by $\cdot$OH. In addition, Cr(VI) can be reduced by surface Fe^{2+} and S^{2-} from the corrosion of S-nZVI during the reaction process [4]. The newly formed Cr(III) and Fe(III) co-precipitate simultaneously on the S-nZVI to form Cr/Fe (oxy)-hydroxide, as per Equations (15) and (16) [35]. The reusability of S-nZVI was further investigated by separating S-nZVI with a magnet after the reaction, followed by washing in deionized water and subsequent reuse for synchronous removal of Cr(VI) and BPA. As presented in Figure S8, BPA can be fully degraded even when S-nZVI was reused three times, but the removal efficiency of Cr(VI) decreased along the number of times that S-nZVI was reused. In the third run, 69.2% of Cr(VI) was removed in the S-nZVI/H_2O_2/Cr/BPA reaction system. The deposition of Fe-Cr oxides impeded the smooth generation of ferrous species from S-nZVI corrosion, leading to a decline in performance for Cr(VI) sequestration.

$$xCr^{3+} + (1 - x)Fe^{3+} + 2H_2O \rightarrow Cr_xFe_{1-x}OOH\downarrow + 3H^+ \tag{15}$$

$$xCr^{3+} + (1 - x)Fe^{3+} + 3H_2O \rightarrow (Cr_xFe_{1-x})(OH)_3\downarrow + 3H^+ \tag{16}$$

After the reaction, a thick iron oxide was formed on the S-nZVI surface, as indicated by the XRD spectrum (Figure S9). Compared to fresh S-nZVI, a new peak appeared at a 2θ angle of 35.6°, which attributed to the facet of hematite (110), implying the formation of iron oxides during the reaction. To better understand the mechanism of BPA elimination and Cr(VI) sequestration, the XPS spectra of S-nZVI were detected before and after the reaction. As shown in Figure 4a, the XPS spectra of Fe 2p on the surface of the pristine S-nZVI at 706.96 eV corresponded to Fe $2p_{3/2}$ of Fe^0 with low content of 2.55% [36]. The binding energies at 712.05 eV and 726.11 eV, coupled with a satellite peak obtained at 719.07 eV and 732.35 eV, respectively, were assigned to Fe $2p_{3/2}$ and Fe $2p_{1/2}$ of Fe (III) in terms of iron (oxy) hydroxide [37]. In addition, the peaks at 710.40 eV and 724.01 eV were attributed to Fe $2p_{3/2}$ and Fe $2p_{1/2}$ of Fe(II), respectively. These results demonstrate that the surface of S-nZVI was slightly oxidized and wrapped by a mixture of Fe(II) and Fe(III), which is consistent with the results of EDX analysis. After the reaction, it can be observed that the peak of Fe^0 disappeared, and the molar ratio of Fe(II) remained nearly unchanged, while the Fe(III) fraction increased from 23.74% to 27.32%, as depicted in Figure 4a and Table S1. Thus, it can be deduced that Fe^0 was sacrificed as the electron donor and converted to Fe(II), which then reacted with Cr(VI) and H_2O_2, resulting in a redox transformation from Fe(II) to Fe(III) [35]. Moreover, four distinguishing peaks can be found in the S2p spectrum (Figure 4b). The binding energies at 161.37 eV and 163.07 eV were attributed to iron monosulfide (FeS) and iron disulfide (FeS$_2$) [38], and the peaks with binding energy of 166.49 eV and 168.42 eV were attributed to SO_3^{2-} and SO_4^{2-}, respectively [39]. After the reaction, the peak intensity of S^{2-} decreased from 56.45% to 14.65% (Table S1), but the peak intensities for SO_3^{2-} and SO_4^{2-} increased remarkably to 6.38% and 78.97%, respectively, demonstrating the involvement of S^{2-} during the reductive adsorption of Cr(VI) and the catalytic activation of H_2O_2 for BPA degradation (Figure 4b). It has been verified that iron sulfides are able to act as good semiconductors or metallic conductors for S-nZVI, thus facilitating the electron transfer from the iron core to the adsorbed contaminants and facilitating the cycle of Fe(II)/Fe(III) [40]. The XPS spectrum of Cr was further tested to confirm the conversion of Cr(VI) to low-toxic Cr(III). After the reaction, as shown in Figure 4c, the deconvolution peaks of Cr 2p at 577.16 eV and 586.76 eV corresponded to Cr_2O_3 [25], and the peaks at 577.37 eV and 587.46 eV were assigned to $Cr(OH)_3$ [41], indicating that Cr(VI) sequestration by S-nZVI was primarily a process of chemisorption, with reduction of Cr(VI) to Cr(III). Additionally, the oxygen peaks with binding energies of 529.72 eV and 531.11eV were assigned to O^{2-} and OH^- (Figure 4d), suggesting the

presence of iron oxide and hydroxyl species of Fe before use, respectively. After the reaction, the content of O^{2-} decreased from 31.98% to 15.65% while the content of OH^- increased from 68.02% to 84.35% (Table S1), indicating the formation of hydroxides on the surface of S-nZVI. These results imply that both $Cr(OH)_3$ and $Cr(III)/Fe(III)$ (oxy)hydroxide were on the surface of S-nZVI after Cr(VI) sequestration. In addition, the atomic fraction of C-C component at a binding energy of 284.8 increased remarkably from 41.83 to 68.19 after the reaction (Figure S10), which may indicate an adventitious organic carbon contamination on S-nZVI surface.
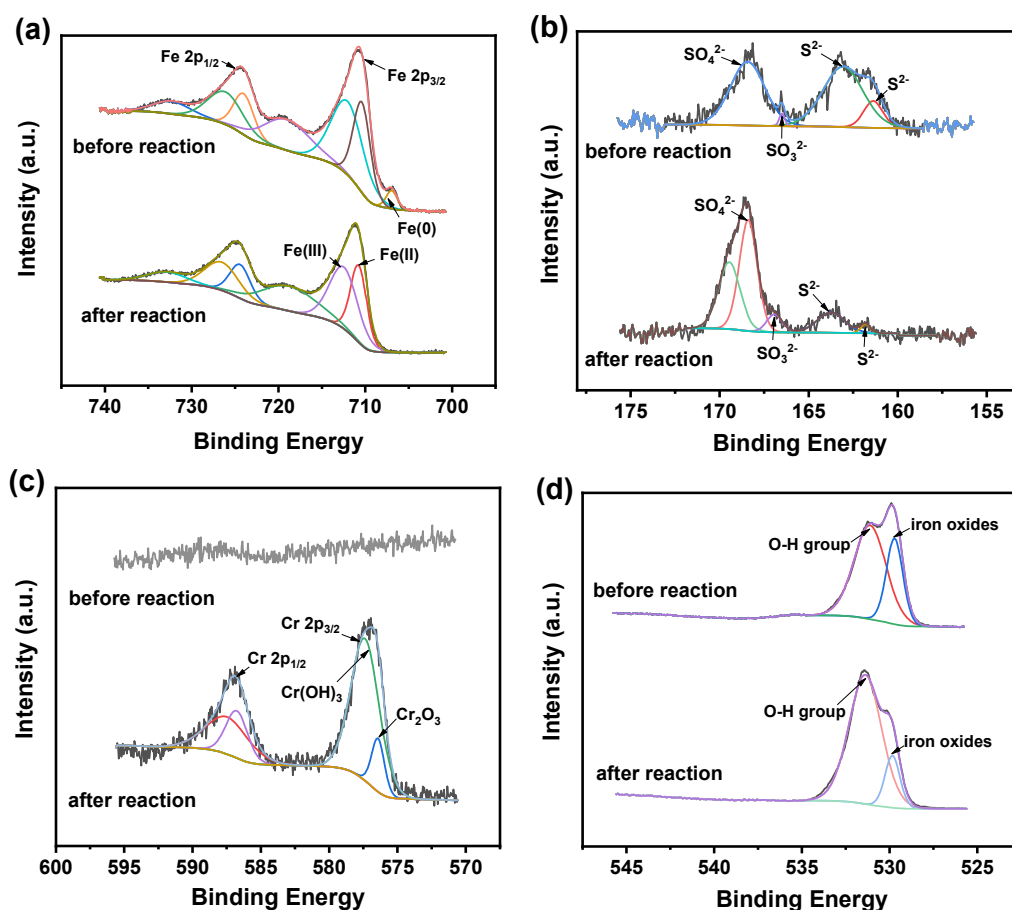

Figure 4. XPS spectra of (**a**) Fe 2p, (**b**) S 2p, (**c**) Cr 2p, (**d**) O 1 s of S-nZVI before and after the reaction.

In summary, a probable mechanism of BPA degradation and Cr(VI) removal by S-nZVI/H_2O_2 system was schematically elucidated, as shown in Figure 5. Under acidic conditions, H_2O_2 was activated by Fe^{2+}, Fe^{3+} and Fe^0 on the S-nZVI surface, producing ·OH for BPA degradation. Interestingly, the co-existence of Cr(VI) negatively slowed the oxidation rate of BPA because of the competitive consumption of H_2O_2 and ·OH. Conversely, the removal of Cr(VI) was positively promoted in the presence of BPA due to its oxidative reaction with ·OH, which inhibited the reoxidation of Cr(III) by ·OH. The stepwise removal of Cr(VI) involved reduction, re-oxidation, adsorption and immobilization. Initially, Cr(VI) was absorbed on the S-nZVI surface and occupied the reactive sites of S-nZVI, and then Cr(VI) was directly reduced to Cr(III) on the S-nZVI surface by Fe^0, Fe(II) and S^{2-}. The dissolved Fe(III) on the surface of S-nZVI could be reduced back to Fe(II) by Fe^0 and S^{2-}, giving rise to more ferrous sites for further Cr(VI) reduction. The produced Cr(III) and Fe(III) were present in the forms of mixed Cr-Fe (oxy) hydroxides, and formed a passivation layer that impeded further reaction. However, it should be highlighted that not all Cr species could be captured by S-nZVI within the reaction time, and a considerable fraction of Cr(VI) was converted directly to Cr(III) through reaction with H_2O_2 under acidic conditions.

The formed Cr(III) presented as dissolved ions at acidic pH, but might sediment further in the form of chromium hydroxides.
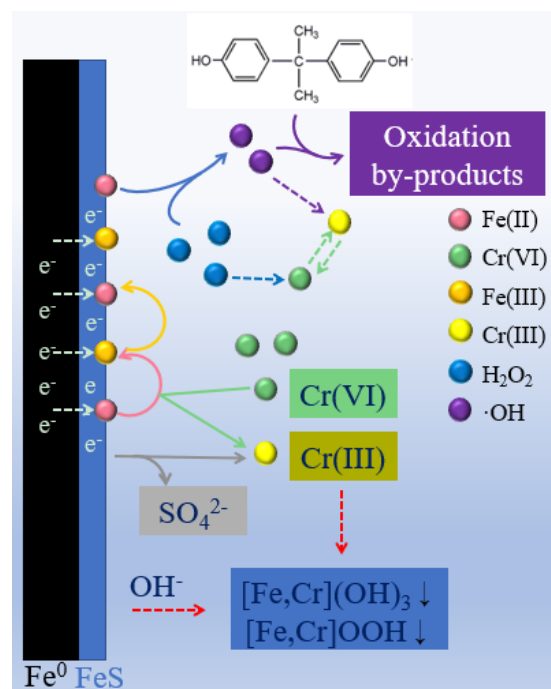

Figure 5. Schematic illustration of synchronous removal of BPA and Cr(VI) in the S-nZVI/H_2O_2 system.

4. Conclusions

The present study used S-nZVI as a reductant and catalyst for heterogeneously activated H_2O_2 for the synchronous removal of BPA and Cr(VI) via processes including both degradation and reductive adsorption. The removal efficiency reached up to 98.2% for BPA and 96.9% for Cr(VI) within 60 min under optimum conditions, which were pH 3, and concentrations of 0.05 g/L of S-nZVI, and 0.2 mmol/L of H_2O_2, respectively. Compared to nZVI/H_2O_2, the S-nZVI/H_2O_2 Fenton-like system showed a very similar efficiency toward BPA degradation, but a faster rate for Cr(VI) removal. HA and $H_2PO_4^-$ inhibited, but NO_3^- promoted the degradation of BPA. This was different from BPA degradation in that the effects of water matrix on Cr(VI) removal were inconspicuous and Cr(VI) could be completely converted to Cr(III) after 30 min reaction time. In addition, ·OH was identified as the principal radical species in the S-nZVI/H_2O_2 Fenton-like system for BPA degradation. However, the reaction with Cr(VI) was a complex process, involving not only reduction by both S-nZVI and H_2O_2, but also ·OH-mediated oxidation of Cr(III). Additionally, the removal of Cr(VI) involved adsorption, reduction and immobilization on the S-nZVI surface, as further evidenced by XPS characterization. This study provides a new feasible solution for the treatment of complex polluted water bodies containing refractory organic pollutants and heavy metal pollutants.

Supplementary Materials: The following supporting information can be downloaded at: https://www.mdpi.com/article/10.3390/catal12030252/s1, Figure S1: Scanning electron micrograph of S-nZVI particles, (a) and (b) Scanning electron microscopy image of S-nZVI, (c) Spectral recording of a spot on S-nZVI image, Figure S2: TEM image of S-nZVI, Figure S3: XRD patterns of nZVI and S-nZVI, Figure S4: TOC removal efficiency in the S-nZVI/H_2O_2/Cr/BPA reaction system, Figure S5: Synchronous removal of (a) BPA and (b) Cr(VI) in systems of S-nZVI/H_2O_2 and S-nZVI/PS, Figure S6: Effect of different conditions on simultaneous removal of BPA and Cr(VI) by S-nZVI; (a) and (b) solution pH; (c) and (d) oxidant dosage; (e) and (f) catalyst dosage, Figure S7: EPR characterization using DMPO, Figure S8: Reusability of S-nZVI for synchronous removal of Cr(VI) and BPA in the S-nZVI/H_2O_2/Cr/BPA reaction system, Figure S9: XRD patterns of S-nZVI before and after the

reaction in the S-nZVI/H_2O_2/Cr/BPA system, Figure S10: XPS spectra of C 1s of S-nZVI before and after the reaction, Table S1: The atomic fraction of each element of S-nZVI before and after the reaction.

Author Contributions: H.L.: Experiments and manuscript organization. X.Z.: Experiments and manuscript writing. T.Z.: Experiments and manuscript writing. F.S.: Experiments. J.B.: Manuscript structure guidance. J.D.: Guidance, review, and editing. All authors have read and agreed to the published version of the manuscript.

Data Availability Statement: Data is contained within the article or Supplementary Material.

Conflicts of Interest: There are no conflicts of interest to declare.

References

1. Barrera-Díaz, C.E.; Lugo-Lugo, V.; Bilyeu, B. A review of chemical, electrochemical and biological methods for aqueous Cr(VI) reduction. *J. Hazard. Mater.* **2012**, *223–224*, 1–12. [CrossRef] [PubMed]
2. Zhao, G.; Sun, Y.; Zhao, Y.; Wen, T.; Wang, X.; Chen, Z.; Sheng, G.; Chen, C.; Wang, X. Enhanced Photocatalytic Simultaneous Removals of Cr(VI) and Bisphenol A over Co(II)-Modified TiO_2. *Langmuir* **2019**, *35*, 276–283. [CrossRef]
3. Dong, F.-X.; Yan, L.; Zhou, X.-H.; Huang, S.-T.; Liang, J.-Y.; Zhang, W.-X.; Guo, Z.-W.; Guo, P.-R.; Qian, W.; Kong, L.-J.; et al. Simultaneous adsorption of Cr(VI) and phenol by biochar-based iron oxide composites in water: Performance, kinetics and mechanism. *J. Hazard. Mater.* **2021**, *416*, 125930. [CrossRef] [PubMed]
4. Zou, H.; Hu, E.; Yang, S.; Gong, L.; He, F. Chromium(VI) removal by mechanochemically sulfidated zero valent iron and its effect on dechlorination of trichloroethene as a co-contaminant. *Sci. Total Environ.* **2019**, *650*, 419–426. [CrossRef]
5. Neyens, E.; Baeyens, J. A review of classic Fenton's peroxidation as an advanced oxidation technique. *J. Hazard. Mater.* **2003**, *98*, 33–50. [CrossRef]
6. Fang, Y.; Yin, W.; Jiang, Y.; Ge, H.; Li, P.; Wu, J. Depth treatment of coal-chemical engineering wastewater by a cost-effective sequential heterogeneous Fenton and biodegradation process. *Environ. Sci. Pollut. Res.* **2018**, *25*, 13118–13126. [CrossRef]
7. Babuponnusami, A.; Muthukumar, K. A review on Fenton and improvements to the Fenton process for wastewater treatment. *J. Environ. Chem. Eng.* **2014**, *2*, 557–572. [CrossRef]
8. Tang, W.Z.; Chen, R.Z. Decolorization kinetics and mechanisms of commercial dyes by H_2O_2/iron powder system. *Chemosphere* **1996**, *32*, 947–958. [CrossRef]
9. Martins, R.C.; Lopes, D.V.; Quina, M.J.; Quinta-Ferreira, R.M. Treatment improvement of urban landfill leachates by Fenton-like process using ZVI. *Chem. Eng. J.* **2012**, *192*, 219–225. [CrossRef]
10. Minella, M.; Sappa, E.; Hanna, K.; Barsotti, F.; Maurino, V.; Minero, C.; Vione, D. Considerable Fenton and photo-Fenton reactivity of passivated zero-valent iron. *RSC Adv.* **2016**, *6*, 86752–86761. [CrossRef]
11. Fu, F.; Dionysiou, D.D.; Liu, H. The use of zero-valent iron for groundwater remediation and wastewater treatment: A review. *J. Hazard. Mater.* **2014**, *267*, 194–205. [CrossRef]
12. Diao, Z.-H.; Xu, X.-R.; Jiang, D.; Liu, J.-J.; Kong, L.-J.; Li, G.; Zuo, L.-Z.; Wu, Q.-H. Simultaneous photocatalytic Cr(VI) reduction and ciprofloxacin oxidation over TiO_2/Fe^0 composite under aerobic conditions: Performance, durability, pathway and mechanism. *Chem. Eng. J.* **2017**, *315*, 167–176. [CrossRef]
13. Yin, X.; Liu, W.; Ni, J. Removal of coexisting Cr(VI) and 4-chlorophenol through reduction and Fenton reaction in a single system. *Chem. Eng. J.* **2014**, *248*, 89–97. [CrossRef]
14. Yang, B.; Zhou, P.; Cheng, X.; Li, H.; Huo, X.; Zhang, Y. Simultaneous removal of methylene blue and total dissolved copper in zero-valent iron/H_2O_2 Fenton system: Kinetics, mechanism and degradation pathway. *J. Colloid Interface Sci.* **2019**, *555*, 383–393. [CrossRef]
15. Diao, Z.-H.; Xu, X.-R.; Chen, H.; Jiang, D.; Yang, Y.-X.; Kong, L.-J.; Sun, Y.-X.; Hu, Y.-X.; Hao, Q.-W.; Liu, L. Simultaneous removal of Cr(VI) and phenol by persulfate activated with bentonite-supported nanoscale zero-valent iron: Reactivity and mechanism. *J. Hazard. Mater.* **2016**, *316*, 186–193. [CrossRef] [PubMed]
16. Diao, Z.-H.; Xu, X.-R.; Jiang, D.; Kong, L.-J.; Sun, Y.-X.; Hu, Y.-X.; Hao, Q.-W.; Chen, H. Bentonite-supported nanoscale zero-valent iron/persulfate system for the simultaneous removal of Cr(VI) and phenol from aqueous solutions. *Chem. Eng. J.* **2016**, *302*, 213–222. [CrossRef]
17. Du, J.; Bao, J.; Lu, C.; Werner, D. Reductive sequestration of chromate by hierarchical FeS@Fe0 particles. *Water Res.* **2016**, *102*, 73–81. [CrossRef]
18. Fontmorin, J.M.; Castillo, R.C.B.; Tang, W.Z.; Sillanpaa, M. Stability of 5,5-dimethyl-1-pyrroline-N-oxide as a spin-trap for quantification of hydroxyl radicals in processes based on Fenton reaction. *Water Res.* **2016**, *99*, 24–32. [CrossRef] [PubMed]
19. Du, J.; Bao, J.; Fu, X.; Lu, C.; Kim, S.H. Mesoporous sulfur-modified iron oxide as an effective Fenton-like catalyst for degradation of bisphenol A. *Appl. Catal. B Environ.* **2016**, *184*, 132–141. [CrossRef]

20. Liu, C.-M.; Diao, Z.-H.; Huo, W.-Y.; Kong, L.-J.; Du, J.-J. Simultaneous removal of Cu^{2+} and bisphenol A by a novel biochar-supported zero valent iron from aqueous solution: Synthesis, reactivity and mechanism. *Environ. Pollut.* **2018**, *239*, 698–705. [CrossRef]

21. Dehghani, M.H.; Heibati, B.; Asadi, A.; Tyagi, I.; Agarwal, S.; Gupta, V.K. Reduction of noxious Cr(VI) ion to Cr(III) ion in aqueous solutions using H_2O_2 and UV/H_2O_2 systems. *J. Ind. Eng. Chem.* **2016**, *33*, 197–200. [CrossRef]

22. Gheju, M.; Iovi, A. Kinetics of hexavalent chromium reduction by scrap iron. *J. Hazard. Mater.* **2006**, *135*, 66–73. [CrossRef] [PubMed]

23. Woo, Y.S.; Rafatullah, M.; Al-Karkhi, A.F.M.; Tow, T.T. Removal of Terasil Red R dye by using Fenton oxidation: A statistical analysis. *Desalin. Water Treat.* **2014**, *52*, 4583–4591. [CrossRef]

24. Guo, S.; Yang, W.; You, L.; Li, J.; Chen, J.; Zhou, K. Simultaneous reduction of Cr(VI) and degradation of tetracycline hydrochloride by a novel iron-modified rectorite composite through heterogeneous photo-Fenton processes. *Chem. Eng. J.* **2020**, *393*, 124758. [CrossRef]

25. Abdul, N.A.; Abdul-Talib, S.; Amir, A. Nano-pyrite as a Reductant to Remove Chromium in Groundwater. *KSCE J. Civ. Eng.* **2019**, *23*, 992–999. [CrossRef]

26. Rehman, F.; Sayed, M.; Khan, J.A.; Shah, N.S.; Khan, H.M.; Dionysiou, D.D. Oxidative removal of brilliant green by $UV/S_2O_8{}^{2-}$, $UV/HSO_5{}^-$ and UV/H_2O_2 processes in aqueous media: A comparative study. *J. Hazard. Mater.* **2018**, *357*, 506–514. [CrossRef]

27. Mak, M.S.H.; Rao, P.; Lo, I.M.C. Effects of hardness and alkalinity on the removal of arsenic(V) from humic acid-deficient and humic acid-rich groundwater by zero-valent iron. *Water Res.* **2009**, *43*, 4296–4304. [CrossRef]

28. Lv, X.; Hu, Y.; Tang, J.; Sheng, T.; Jiang, G.; Xu, X. Effects of co-existing ions and natural organic matter on removal of chromium (VI) from aqueous solution by nanoscale zero valent iron (nZVI)-Fe_3O_4 nanocomposites. *Chem. Eng. J.* **2013**, *218*, 55–64. [CrossRef]

29. Zhang, R.; Sun, H.; Yin, J. Arsenic and chromate removal from water by iron chips—Effects of anions. *Front. Environ. Sci. Eng. China* **2008**, *2*, 203–208. [CrossRef]

30. Ma, J.; Yang, Y.; Jiang, X.; Xie, Z.; Li, X.; Chen, C.; Chen, H. Impacts of inorganic anions and natural organic matter on thermally activated persulfate oxidation of BTEX in water. *Chemosphere* **2018**, *190*, 296–306. [CrossRef]

31. Døssing, L.N.; Dideriksen, K.; Stipp, S.L.S.; Frei, R. Reduction of hexavalent chromium by ferrous iron: A process of chromium isotope fractionation and its relevance to natural environments. *Chem. Geol.* **2011**, *285*, 157–166. [CrossRef]

32. Funahashi, S.; Uchida, F.; Tanaka, M. Reactions of hydrogen peroxide with metal complexes. 3. Thermodynamic and kinetic studies on the formation, dissociation and decomposition of peroxochromium(VI) complexes in acid media. *Inorg. Chem.* **1978**, *17*, 2784–2789. [CrossRef]

33. Watwe, V.S.; Kulkarni, S.D.; Kulkarni, P.S. Cr(VI)-Mediated Homogeneous Fenton Oxidation for Decolorization of Methylene Blue Dye: Sludge Free and Pertinent to a Wide pH Range. *ACS Omega* **2021**, *6*, 27288–27296. [CrossRef] [PubMed]

34. Gong, Y.; Gai, L.; Tang, J.; Fu, J.; Wang, Q.; Zeng, E.Y. Reduction of Cr(VI) in simulated groundwater by FeS-coated iron magnetic nanoparticles. *Sci. Total Environ.* **2017**, *595*, 743–751. [CrossRef]

35. Song, X.; Ren, C.; Zhao, Q.; Su, B. Simultaneous removal of Cr(VI) and triclosan from aqueous solutions through Fe_3O_4 magnetic nanoscale-activated persulfate oxidation. *Chem. Eng. J.* **2020**, *381*, 122586. [CrossRef]

36. Sun, Y.-P.; Li, X.-Q.; Cao, J.; Zhang, W.-X.; Wang, H.P. Characterization of zero-valent iron nanoparticles. *Adv. Colloid Interface Sci.* **2006**, *120*, 47–56. [CrossRef]

37. Jeong, H.Y.; Han, Y.-S.; Park, S.W.; Hayes, K.F. Aerobic oxidation of mackinawite (FeS) and its environmental implication for arsenic mobilization. *Geochim. Cosmochim. Acta* **2010**, *74*, 3182–3198. [CrossRef]

38. Rajajayavel, S.R.C.; Ghoshal, S. Enhanced reductive dechlorination of trichloroethylene by sulfidated nanoscale zerovalent iron. *Water Res.* **2015**, *78*, 144–153. [CrossRef]

39. Pratt, A.R.; Muir, I.J.; Nesbitt, H.W. X-ray photoelectron and Auger electron spectroscopic studies of pyrrhotite and mechanism of air oxidation. *Geochim. Cosmochim. Acta* **1994**, *58*, 827–841. [CrossRef]

40. Zhu, X.; Le, T.T.; Du, J.; Xu, T.; Cui, Y.; Ling, H.; Kim, S.H. Novel core-shell sulfidated nano-Fe(0) particles for chromate sequestration: Promoted electron transfer and Fe(II) production. *Chemosphere* **2021**, *284*, 131379. [CrossRef] [PubMed]

41. Biesinger, M.C.; Lau, L.W.M.; Gerson, A.R.; Smart, R.S.C. Resolving surface chemical states in XPS analysis of first row transition metals, oxides and hydroxides: Sc, Ti, V, Cu and Zn. *Appl. Surf. Sci.* **2010**, *257*, 887–898. [CrossRef]